A LIMITED -SCALE EXPEIRMENTAL INVSTIGATION OF THE UNIT CELL TOPOLOGY EFFECTS ON INTERPENETRATING CELLULAR STRUCTURES

Matthew Roe*, Li Yang*

*Department of Industrial Engineering, University of Louisville, Louisville, KY 40292

Abstract

The interpenetrating cellular structure is a novel recent design concept that has been subjected to some preliminary research efforts in recent years. As there still exist relatively limited understanding of such design concept, the current work aimed to provide additional insights via experimental-based study. Several baseline cellular unit cell structures that follow multiple cellular unit cell topology design rules were included in the study, in order to investigate whether there exist significant design relationships between the cellular topology pairing and the resulting performance of the interpenetrating structures. In general, the interpenetrating designs did not result in synergetic performance reinforcement with elastic modulus, ultimate strength or energy absorption, except for specific cases. In most cases, the local strut interaction between the two component cellular structures appear to exert negative effects on the properties of the interpenetrating structures. The results tentatively suggest the need of additional research with such concept.

Keywords: Interpenetrating design, cellular structure, design, experimentation investigation

Introduction

In the broad research area of cellular structure design, interpenetrating cellular design appears to be an interesting new concept that has drawn some research interests in the past several years. The concept of interpenetrating cellular design can be perhaps considered similar to multiple well-known design concepts with materials and structures, including composites, woven textiles and semiconductors with superlattices. From the perspective of the design architecture, an intuitive definition of interpenetrating cellular design was given by White et al. as two or more directly non-connected cellular structures that interweave through the same bounding volume [1]. The interpenetrating design concept has been demonstrated in the design of novel polymer materials, as demonstrated in multiple literatures [2, 3]. It was suggested that the interpenetrating molecular structure design could serve as an effective method for toughening of polymer materials [4]. At macroscopic/structural level, the concept of interpenetrating structure is commonly seen with woven textile products, in which yarns of different colors or materials are interwoven into complex 2D or 3D patterns. The definition provided by White et al. [1] also implies that the interpenetrating designs can be represented conveniently by representative volume element (EVE), or unit cell. Therefore, cellular structures appear to be intuitive candidates for the component design of the interpenetrating structures. Cellular structures exhibit 3D interconnected porosities and 3D connectivity, and can be custom-designed to exhibit a broad range of mechanical and physical properties. There exist extensive knowledge body for the design of cellular structures, as well as a vast number of specific topology designs for different performance objectives. Therefore there might exist extensive design potentials with the cellular structure-based interpenetrating designs.

There currently exists limited literatures on the design potentials of the interpenetrating cellular designs. White et al. investigated an interpenetrating design that is constructed from a face center cubic (FCC) unit cell and a rhombic dodecahedron (RD) unit cell, as shown in Fig.1a [1]. It was suggested that such design concept could potentially results in improved damage tolerance with the interpenetrating structures by overcoming the catastrophic failure mode associated with individual component structures. It was also suggested that the design concept can be exploited for thermal conductivity design by adjusting the per-

volume strut connectivity, although further details are yet to be reported. Another exploratory study by Do et al. investigated the interpenetrating cellular design for adjustable fluid flow control [5]. The design was constructed by two interpenetrating diamond lattices with their spatial offset the adjustable variable for flow control, as shown in Fig.1b [5]. It was shown both experimentally and theoretically that variable pressure drop and cavity mode could be achieved via the adjustment of unit cell size and strut diameter.

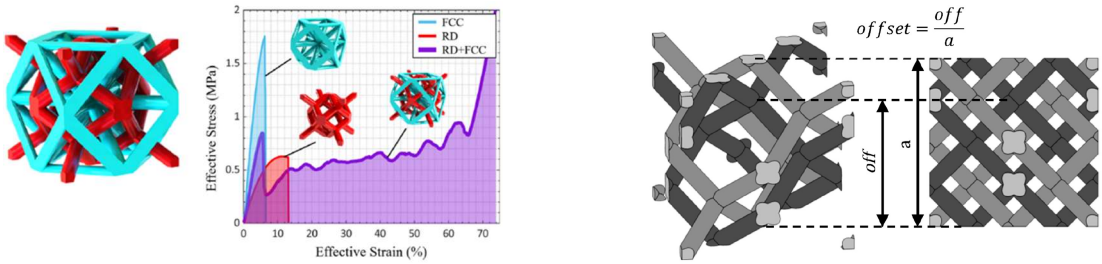

a. FCC+RD design for energy absorption [1] b. Diamond+diamond design for flow control [5]

Fig.1 Exploratory designs of interpenetrating cellular structures from literature

Depending on how the two components interact with each other, the interpenetrating designs could be roughly categorized into three different types, including full-contact, partial-contact and non-contact. Woven textile structures are examples of full-contact interpenetrating structures. With increased level of component interaction, the behaviors of the interpenetrating structures also become more complex, and contact-based mechanisms such as friction, heat transfer and mechanical interlocking could occur. These mechanisms have been shown to significantly enhance certain performance of the structures [5.1], therefore hold promising potentials in a broad range of future applications. s

A potentially valuable question is whether there exist any design rules for the interpenetrating cellular designs. White et al. suggested the use of multiple geometry definitions for the cellular designs such as connectivity, relative density and unit cell geometry dimensions, which are well-established from classic cellular design theories [1]. Additional design variables for the design of the relative relationships between the two interpenetrating components, such as the relative orientation of the two unit cells and their interaction types (e.g. contacting, partially connected, separating), were also suggested to be significant but not investigated [1]. Another important aspect is the dimensional scale of the interpenetration structures. The interaction of the structure with a field (e.g. acoustic, electromagnetic) with specific wavelength spectra is heavily dependent on the characteristic dimensions of the structure [6]. In the design of cellular-based metamaterials, the topology design of the metamaterials could significantly influence the coupling of the structures with the field and consequently the characteristic behaviors. With interpenetrating design, additional freedoms with the design of behaviors and characteristics could potentially be realized. In addition, with reduced dimensional scale, structures and materials exhibit shifting behaviors due to the increased significance of surface-based mechanisms and short-distance interactions, such as Van der Waals force and surface tension, which also render often unexpected and attractive behaviors with the structures. Various such examples for interpenetrating cellular designs can be found in the design of novel polymers with interpenetrating molecular structures [7].

In this study, efforts were focused on the investigation of the effects of cellular structure design rules on the characteristics of the non-contact type of interpenetrating cellular structures. It was hypothesized that the existing cellular structure design rules, including the dominant deformation mode, the auxeticity, and the presence of buckling mode, could be utilized to guide the interpenetration designs. The study was mainly carried out experimentally with limited finite element analysis, and although the observations were not considered conclusive or comprehensive, such design rule-based study with the cellular geometry designs was considered to potentially provide more representative results to a range of cellular designs.

Designs and experimental procedures

In theory there exist infinite possible topology designs of cellular unit cell geometries even with just one single type of geometry bounding volume. Therefore, it is often more effective to design based on certain guidelines or rules. For periodic strut-based cellular structures, which have been subjected to more extensive studies, several design rules have been identified from the literatures:

1. Dominant deformation mode: For strut-based cellular structures, as the strut elements can be approximated as classic beam elements, their dominant deformation mode could be classified into bending-dominated and stretching-dominated types. Bending-dominated structures generally exhibit lower elastic modulus and strength, as well as "smoother" post-yield behaviors. On the other hand, stretching-dominated structures tend to exhibit higher elastic modulus and strength, as well as a more significant post-failure softening behavior. One of the most commonly employed design criteria for the dominant deformation mode is the Maxwell criterion [8].
2. Auxeticity: Structures that exhibit auxetic behaviors, i.e. negative Poisson's ratios, generally exhibit significantly different properties compared to non-auxetic designs, such as enhanced shear modulus and shear strength, as well as favorable energy absorption capabilities [9].
3. Presence of buckling mode: Elastic buckling of strut is a significant mode of failure of structures, and generally leads to abrupt change of the status of the structures. While this could be potentially utilized to design for multi-status cellular structures [10], it is typically undesirable in the design of ultimate strength as it could often cause catastrophic failure.

For this study, it was of interest to introduce cellular design combinations of different rules into the investigation. A rather intuition manual geometry design process was utilized to devise the different types of representative unit cell geometries. It should be noted that a specific cellular structure designs can be classified by all the design rules, and therefore it can be difficult to investigate the effect of a single design rule in isolated way. Another factor is the topology interference between the two components. For non-contact interpenetrating designs, the requirement that there exists certain spatial clearance between the two cellular components imposes restrictions on the geometry designs of certain types of geometries such as the stretching-dominated structures, which have higher degree of spatial connectivity.

As shown in Fig.2, four different types of unit cells were included in this study, including the re-entrant auxetic (Aux), BCC, BCC with vertical strut (BCC-V) and BCC with horizontal strut (BCC-H). The re-entrant auxetic design exhibits negative Poisson's ratios and bending dominated deformation mode, the BCC exhibit positive Poisson's ratio and bending dominated deformation mode. Both BCC-V and BCC-H were expected to exhibit more rigid beam stretching/compression behaviors due to the inclusions of additional struts compared to BCC, but are still both bending dominated designs. Two unit cell designs, namely the re-entrant auxetic and the BCC-V, exhibit the presence of buckling mode. Note that buckling mode was not investigated as an active design rule in this study, and was instead only noted during the analysis with the results. Furthermore, in order to establish all the feasible combinations of dominated deformation mode and auxeticity. Additional variation in the patterning of some of the unit cells were incorporated in the experimental design. Both the BCC and BCC-V were patterned in two different ways. As illustrated in Fig.3, the first pattern configuration follows the symmetry of the minimum geometry bounding volume, whereas the second pattern follows the axes defined by the two extension directions of the "butterfly wing" features. The two configurations were expressively termed "BCC-V" and "BCC-E-V" for the BCC-V design, and "BCC" and "BCC-E" for the BCC unit cell design.

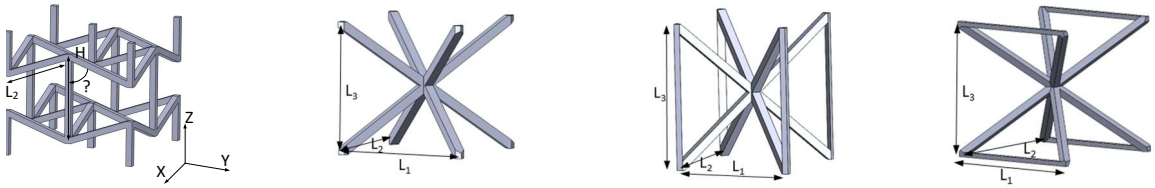

a. Re-entrant auxetic (Aux) b. BCC c. BCC-V d. BCC-H

Fig.2 Design of unit cells

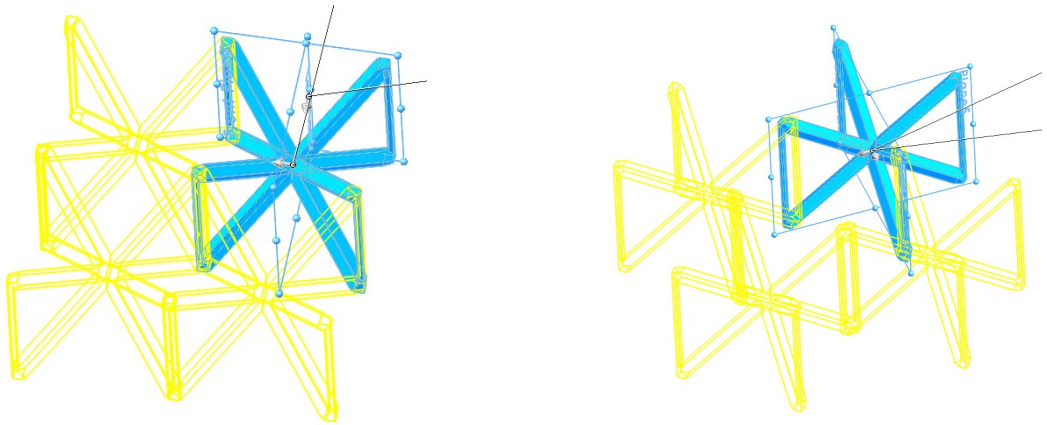

a. Pattern configuration 1 b. Pattern configuration 2

Fig.3 Pattern of BCC-V and BCC-E-V unit cells (showing BCC-V as example)

5 interpenetrating structures were designed, which represent different combinations of the auxeticity and dominated deformation mode. Fig.4 shows the final cellular structure component designs, and Fig.5 illustrates the interpenetrating designs. The auxetic + auxetic interpenetrating design was not included in the experimental design as no other auxetic unit cell design that could establish non-interfering interpenetrating configuration with the re-entrant auxetic design was identified at the time of the experiment. The geometry parameters of the unit cells of all the designs were rather arbitrarily selected, with the only design objective of ensuring relatively consistent relative densities of about 0.05 and overall unit cell sizes. Detailed geometry design parameters are listed in Table 1. For the cellular components, a cellular pattern size of 4x4x4 was used for all designs.

a. Re-entrant auxetic b. BCC-H

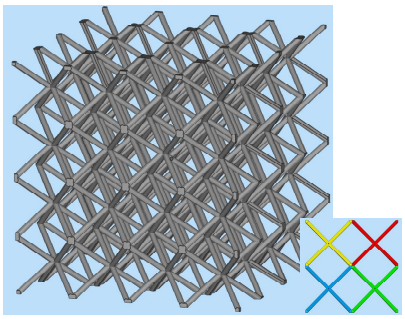

c. BCC

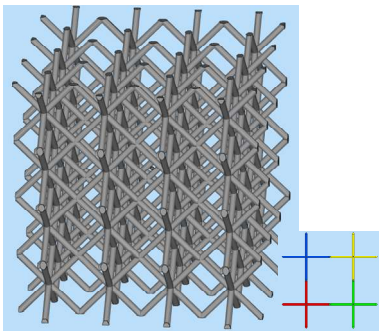

d. BCC-E

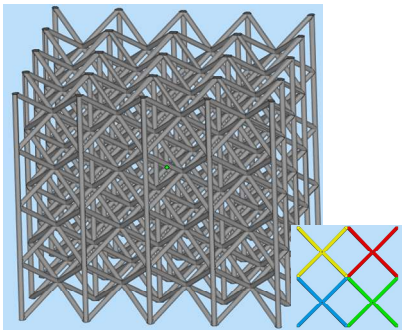

e. BCC-V

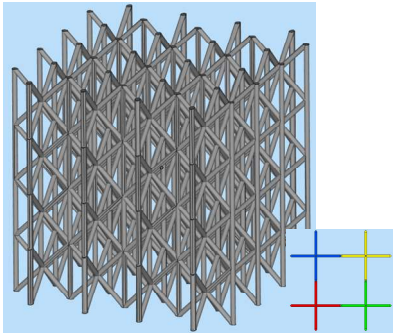

f. BCC-E-V

Fig.4 Cellular component designs

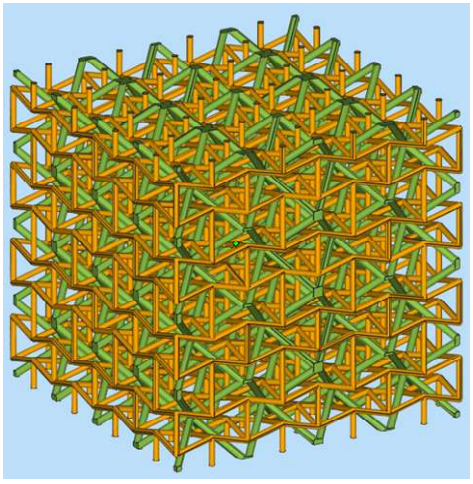

a. Aux+BCC

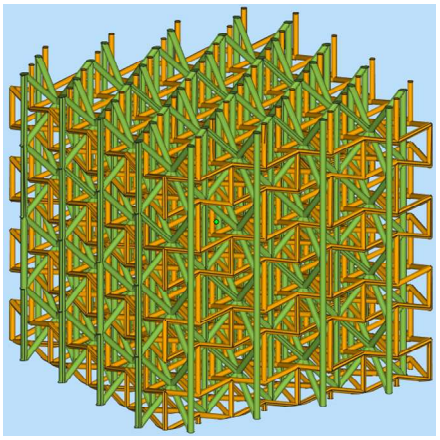

b. Aux+BCC-E-V

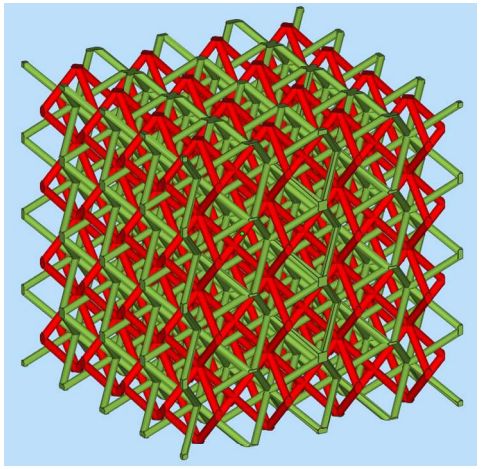

c. BCC+BCC-E

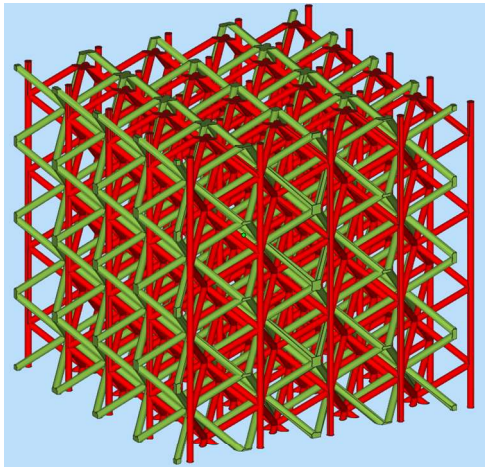

d. BCC+BCC-V

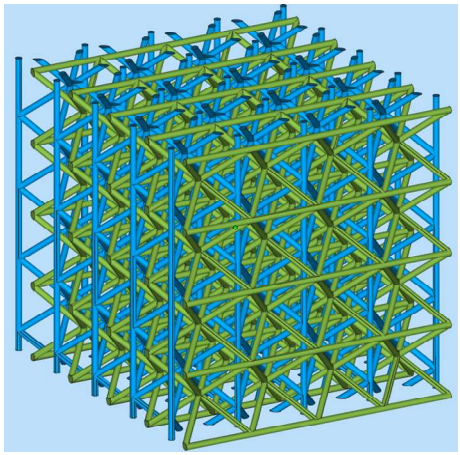

e. BCC-V+BCC-H

Fig.5 Interpenetrating designs

Design	L_1/H (mm)	L_2/L (mm)	L_3 (mm)/θ	t (mm)	Relative density
Aux	9.51	7.76	75°	1.077	0.057
BCC	15	15	14.99	1.437	0.057
BCC-E	11.31	11.31	14.99	1.584	0.055
BCC-V	15	15	14.99	1.284	0.050
BCC-E-V	11.31	11.31	14.99	1.315	0.045
BCC-H	15	15	14.99	1.284	0.050

Table 1 Geometry design parameters for unit cells

With cellular component relative density of about 0.05, the relative densities of the interpenetrating designs were expected to be 0.10 due to the approximately identical geometry bounding volume sizes with all the cellular components (~60mmx60mmx60mm).

The designs were fabricated by an HP MultiJet Fusion 4200 system using system-standard nylon 12 as material. The process setting with the system was controlled by the processing software, and were neither accessible nor visible to users. All the samples were oriented carefully to ensure consistent orientation among the same cellular topology designs. 4-5 samples were fabricated for each of the cellular components as well as the interpenetrating designs.

After sample cleaning, the overall dimensions and weights of the samples were measured. The purpose of this characterization was to both evaluate the relative density of the structures and to estimate the process quality consistency with the samples. Afterwards, the samples were subjected to compressive testing with an Instron 5569A universal tensile testing system. The samples were sandwiched between the two platens and compressed at 1mm/s rate until a total of 0.5 total strain, which was still significantly lower than the densification strain levels for all the designs. In the calculation of mechanical properties, the yield point was estimated utilizing the second-derivative method previously described by Chrisensen [11]. The total energy absorption was calculated based on the stress-strain curve up to 0.5 of strain for each sample.

Results and discussions

The dimensions, weights and calculated relative densities of the fabricated samples are listed in Table 2. In general the dimensional accuracy of the samples were considered adequate and consistent. The relative densities of all the designs were consistently lower than the designs, which was mainly caused by the smaller strut diameters of the fabricated samples. As the deviations were generally consistent, it was not considered a significant issue for the purpose of this study and was not further investigated.

Design	D1 (mm)	D2 (mm)	D3 (mm)	Weight (g)	RD
Aux	60.875±0.126	60.75±0311	59.825±0.275	6.86±0.60	0.031±0.003
BCC	59.750±0.379	60.150±0.311	59.825±0.096	7.49±0.06	0.035±0.000
BCC-E	61.600±0.141	61.475±0.222	59.850±0.208	8.03±0.19	0.035±0.001
BCC-V	61.650±0238	61.850±0.191	60.275±0.222	7.14±0.07	0.031±0.000
BCC-H	60.250±0.379	61.276±0.250	62.050±0.412	7.22±0.16	0.031±0.000
BCC-E-V	60.200±0.082	60.325±0.126	60.050±0.129	6.93±0.08	0.031±0.000
Aux+BCC	61.100±0.115	61.125±0.171	59.700±0.216	13.96±0.21	0.062±0.001
Aux+BCC-E-V	63.675±0.457	63.275±0.544	60.125±0.096	12.97±0.23	0.053±0.001
BCC+BCC-E	60.325±0.538	60.550±0.379	60.350±0.311	15.68±0.35	0.070±0.001
BCC+BCC-V	64.750±0.379	61.500±0.707	60.750±0.420	15.56±0.09	0.064±0.001
BCC-H+BCC-V	67.125±0.298	62.000±0.432	61.700±0.346	15.98±0.36	0.062±0.001

Table 2 Geometry characterization of fabricated samples

The stress-strain curves for the stand-alone cellular components are shown in Fig.6, and the mechanical properties including elastic modulus, yield strength, maximum strength and total energy absorption are shown in Table 3.

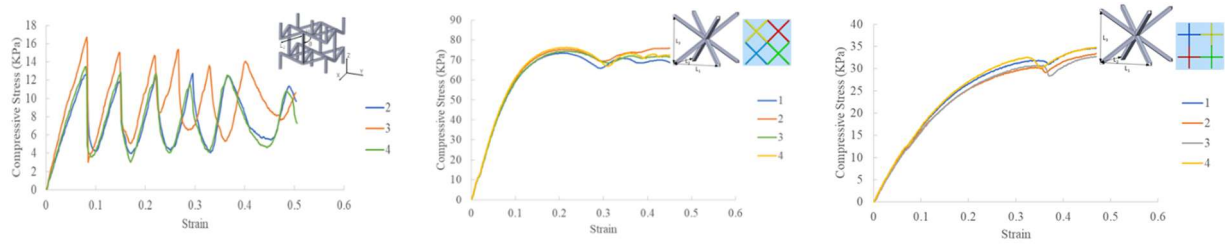

a. Aux b. BCC c. BCC-E

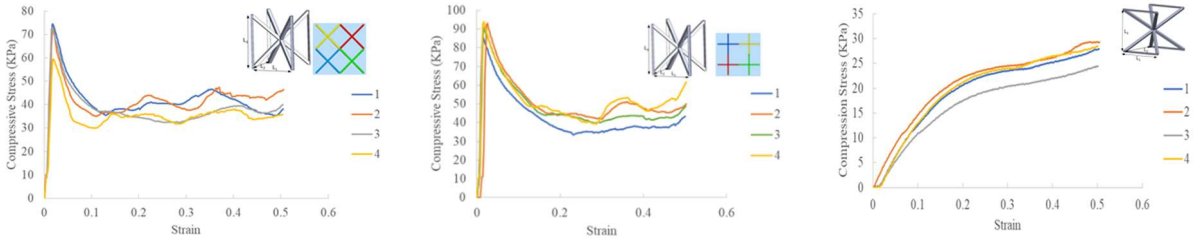

d. BCC-V e. BCC-E-V f. BCC-H

Fig.6 Stress-strain curves for the stand-alone cellular components

	Aux	BCC	BCC-E	BCC-V	BCC-H	BCC-E-V
E (MPa)	0.194±0.028	0.163±0.006	0.722±0.021	6.439±0.802	0.110±0.013	10.910±0.233
YS (MPa)	0.009±0.001	0.016±0.001	0.033±0.003	0.070±0.007	0.018±0.002	0.095±0.003
Max. Strength (MPa)	0.014±0.002	0.031±0.001	0.072±0.002	0.070±0.007	0.027±0.002	0.095±0.003
Energy absorption (J)	0.898±0.114	2.669±0.070	6.978±0.148	4.554±0.374	2.199±0.195	5.473±0.409

Table 3 Mechanical properties of the stand-alone cellular components

The stress-strain curves of the cellular components exhibit consistent characteristics to most of the literature. With the re-entrant auxetic structure, due to the presence of the primary load-bearing vertical struts that could be subjected to buckling failure, as well as the auxetic design, the structures exhibit rather catastrophic layerwise failure pattern, which corresponds to the observed stress fluctuation. The BCC-V and BCC-E-V structure exhibited very high elastic modulus and post-yield softening behaviors, which resemble those of a strength-dominated design. Such behavior was mainly attributed to the buckling failure of the vertical struts within these structures. On the other hand, the BCC-H structure exhibited more bending-dominated-type behaviors instead of the intended rigid stretch-dominated design-like behaviors. This was largely due to the high ductility of the nylon 12 material, which allowed for the hinging-yielding-type failure with the tilted struts that dominated the overall behaviors of the structures. As an additional note, despite the general notion that auxetic structures exhibit higher energy absorption capability, due to the large fluctuation of stress-strain curve patterns, the re-entrant auxetic structures did not exhibit high energy absorption.

The representative stress-strain curves of the interpenetrating designs are shown in Fig.7, along with the stress-strain curves of the corresponding cellular components. The mechanical properties of the interpenetrating designs are listed in Table 4.

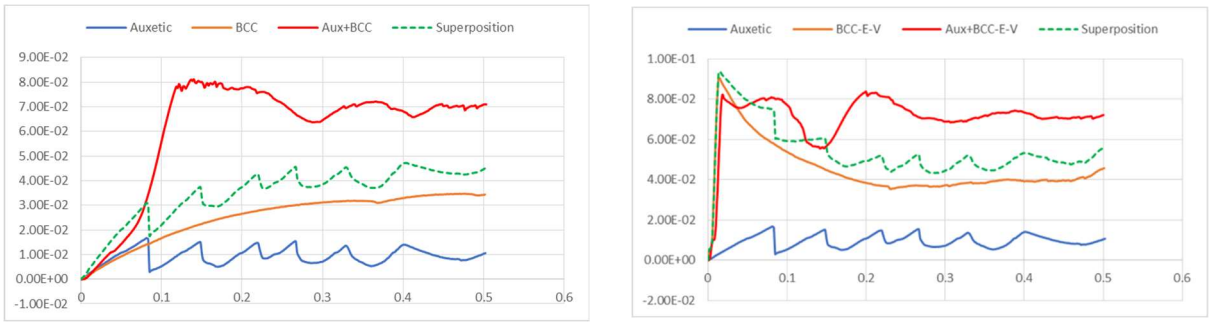

a. Aux+BCC b. Aux+BCC-E-V

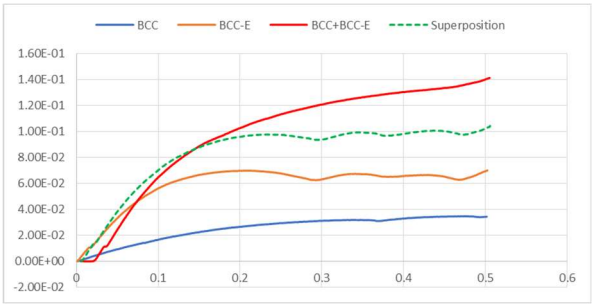

c. BCC+BCC-E

d. BCC+BCC-V

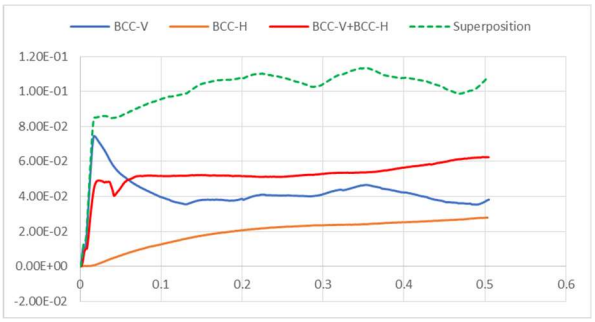

e. BCC-V+BCC-H

Fig.7 Representative stress-strain curves for the interpenetrating cellular designs

Design	Aux+BCC	Aux+BCC-E-V	BCC+BCC-E	BCC+BCC-V	BCC-V+BCC-H
E (MPa)	0.462±0.015	8.834±0.557	0.907±0.058	5.511±0.353	4.942±1.042
YS (MPa)	0.031±0.001	0.079±0.003	0.045±0.006	0.067±0.003	0.047±0.010
Max. Strength (MPa)	0.082±0.002	0.079±0.003	0.142±0.002	0.068±0.002	0.052±0.010
Energy absorption (J)	6.676±0.153	8.326±0.362	10.839±0.319	8.120±0.155	6.885±0.176

Table 4 Mechanical properties of the interpenetrating designs

For the non-contacting interpenetrating designs, it was expected that in the initial elastic deformation stage the behaviors of the two cellular components are largely independent. After certain amount of strain, the two components will get into contact and start to behave in gradually increasingly interacted manner. Therefore, in addition to the stress-strain curves of the interpenetrating designs and their components, an imaginary stress-strain curve from the linear superposition of the two component stress-strain curves was also included in each of the curves in Fig.7 for reference.

From the results, the interpenetrating designs that contain re-entrant auxetic components exhibit overall more significant increase of overall plateau strength. The overall strength of the interpenetrating structures are higher than the linear superposition effect, which suggests that there exist some “positive synergetic” effects between the two components. The large stress fluctuation characteristic to the re-entrant auxetic structures becomes largely absent, which could be contributed to the more smooth post-yield responses of the other component. On the other hand, the mechanical strength of the interpenetrating designs appears to be approximate to linear superposition. Lastly, for the design with BCC-V and BCC-H, the interpenetrating design exhibited relatively insignificant strength enhancement compared to the stronger of the two components (BCC-V).

Considering that the interpenetrating designs do exhibit higher relative densities compared to their components, it is necessary to establish further analysis to evaluate the significance of the "synergetic" effect through the design. As the designs investigated in this study were non-contacting, a relatively simple analytical modeling-based analysis could potentially provide the information needed. As shown in Fig.8, for an arbitrary interpenetrating design under the boundary condition of a nominal uniaxial stress σ_0 on one platen along the principal axial direction and the other platen fully constrained, a uniaxial deformation Δ_0 is introduced. As both component structures C_1 and C_2 are bonded to the same boundary platens, they are subjected to the same uniaxial deformation as a result.

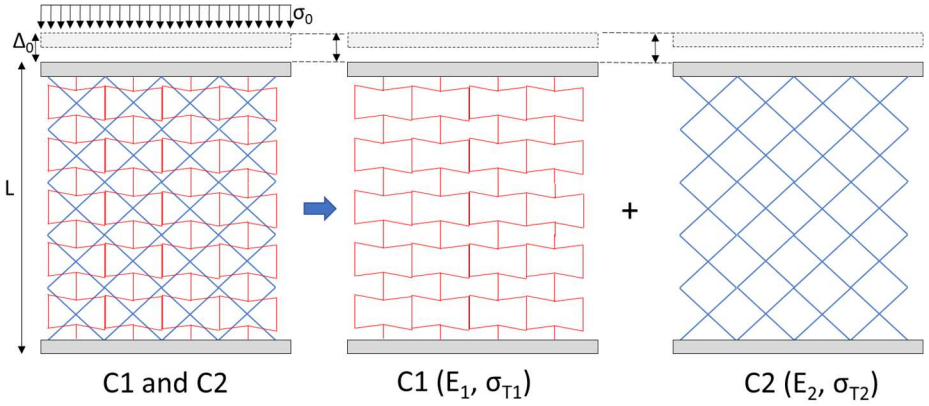

Fig.8 Modeling of interpenetration designs

Define the elastic modulus and yield strength of each of the component cellular structures C_1 and C_2 as E_1, σT_1 and E_2, σT_2, respectively. Assume linear elasticity before yielding, upon deformation Δ_0, the boundary stress level of cellular components C_1 and C_2, or $\sigma 1$ and $\sigma 2$ respectively, are:

$$\sigma_1 = \frac{\Delta_0}{L} E_1 \qquad (1.1)$$

$$\sigma_2 = \frac{\Delta_0}{L} E_2 \qquad (1.2)$$

Therefore, the total boundary stress level for the interpenetrating cellular designs satisfies:

$$\sigma_0 = \sigma_1 + \sigma_2 = \frac{\Delta_0}{L}(E_1 + E_2) \qquad (2)$$

Therefore, the elastic modulus of the interpenetrating structure E is:

$$E = \frac{\sigma_0}{\varepsilon_0} = \frac{\Delta_0}{L}(E_1 + E_2) \cdot \frac{L}{\Delta_0} = E_1 + E_2 \qquad (3)$$

where ε_0 is the strain of the structure. It is noted that $\varepsilon_0 = \varepsilon_1 = \varepsilon_2$.

As the initial yield of the structure could still be considered as within the perfectly elastic domain, it could also be modeled and estimated. The yield strength of the interpenetrating design is expected to be determined by the weaker of the two component structures. Due to linear elasticity assumption, the weaker component structure could be identified via:

$$\min_{Index(1,2)}\left(\frac{\sigma_{T1}}{\sigma_1},\frac{\sigma_{T2}}{\sigma_2}\right)=\min_{Index(1,2)}\left(\frac{L\sigma_{T1}}{\Delta_0 E_1},\frac{L\sigma_{T2}}{\Delta_0 E_2}\right)=\min_{Index(1,2)}\left(\frac{\sigma_{T1}}{E_1},\frac{\sigma_{T2}}{E_2}\right) \tag{4}$$

Once the critical component structure is identified, the yield strength of the interpenetrating structure can be determined through Eq.(1), Eq.(2) and Eq.(4) as:

$$\begin{aligned}\sigma_T &= \frac{\sigma_{Ti}}{\sigma_i}\sigma_0=\frac{\sigma_{Ti}}{E_i\varepsilon_i}\sigma_0=\frac{L\sigma_{Ti}}{E_i\Delta_0}\sigma_0=\frac{L\sigma_{Ti}}{E_i\Delta_0}\cdot\frac{\Delta_0}{L}(E_1+E_2)\\ &=\frac{E_1+E_2}{E_i}\sigma_{Ti}\quad (i=1,2)\end{aligned} \tag{5}$$

Based on Eq.(3) and Eq.(5), the elastic modulus of the non-contacting interpenetrating cellular designs from this study is simply the summation of the elastic modulus of the two components, whereas the yield strength is determined as a linear extrapolation of the weaker component based on elastic modulus.

The comparison of the elastic modulus of the interpenetrating designs versus the summation of the two components are compared in Fig.9a, and the comparison of the initial yield strength of the interpenetrating designs versus the theoretical predictions per Eq.(5) are shown in Fig.9b. From Fig.9a, none of the interpenetrating designs exhibited the linear summation elastic modulus characteristic. The Aux+BCC design was the only one that exhibited higher elastic modulus than the summation of the two components, whereas for the other designs the elastic modulus are lower than the summation of the two components. This was a puzzling observation, and it was suspected that despite the design intention, there exist some initial contact between the two components with the interpenetrating cellular designs. To verify such hypothesis, an additional finite element analysis (FEA) was carried out using SolidWorks Simulation using a random material. The problems were set up as perfectly-elastic problems, and the compressive properties of the interpenetrating designs as well as individual components were evaluated. Fig.10 shows the results of elastic modulus for all the interpenetrating designs. The only design that exhibited linear summation characteristics was the Aux+BCC. It was therefore concluded that although there exist some likely experimental configuration issues that introduced errors in the estimation of elastic modulus, the lack of linear superposition characteristic with the elastic modulus with the interpenetrating cellular structures appears to exist, which calls for additional scrutiny with the experimental design and the results.

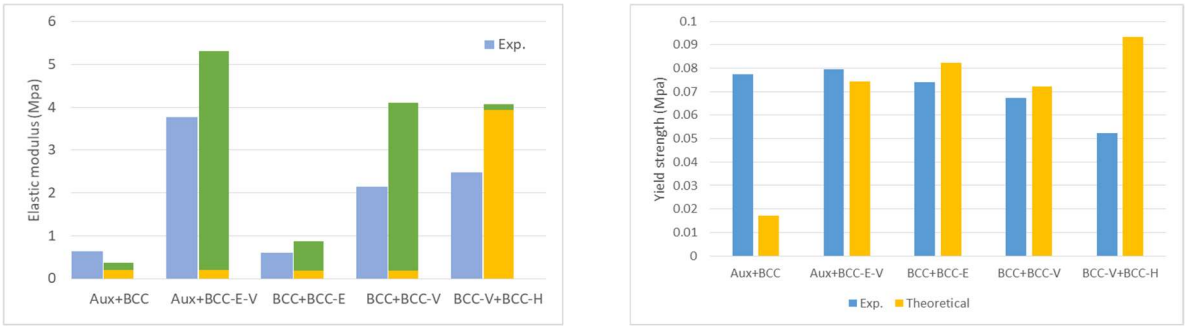

a. Elastic modulus b. Initial yield strength

Fig.9 Comparison of theoretical prediction versus experimentation for interpenetrating cellular designs

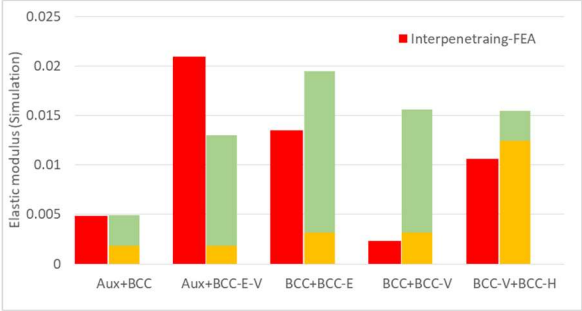

Fig.10 FEA of elastic modulus of the interpenetrating cellular designs

Conclusions

In this work, a preliminary experimental study was carried out to evaluate the mechanical properties of the interpenetrating cellular structure designs with non-contacting cellular components. Five types of cellular structure patterns, including re-entrant auxetic, BCC, BCC with pattern variation, BCC-V, BCC-V with pattern variation, and BCC-H, were investigated. These cellular structures represent different design rule combinations that are well-established for cellular structure designs. Five Interpenetrating designs with the combinations of different cellular rule combinations were created using polymer powder bed fusion and experimentally characterized. The experimental results suggest that the cellular design rules, including the dominate deformation mechanism and auxeticity, appear to exert significant effects in the overall performance of the interpenetrating structures, although the actual effects differ from the classic theories. Despite the theoretical prediction, the elastic modulus of the non-contact interpenetrating cellular structures does not appear to follow the linear superposition rule, which requires further investigation to verify. Within the design space investigated in this study, the re-entrant auxetic cellular structures appear to be a beneficial component for the interpenetrating designs by introducing enhanced mechanical properties to the structure.

Acknowledgement

The authors are grateful of the support of the sample fabrication and experimentation from the Additive Manufacturing Institute of Science and Technology (AMIST) Center at University of Louisville.

References

[1] B. C. White, A. Garland, R. Alberdi, B. L Boyce. Interpenetrating lattices with enhanced mechanical functionality. Additive Manufacturing. 38(2021): 101741.
[2] S. Krishnamoorthy, Z. Zhang, C. Xu. Biofabricatin of three-dimensional structures based on gelatin methacrylate-alginate interpenetrating network hydrogel. Journal of Biomaterials Applications. 33(2019), 8: 1105-1117.
[3] C. J. Dionne, M. A. Rahman, p. E. Hopkins, A. Giri. Spremolecular interactions lead to remarkably high thermal conductivities in interpenetrated two-dimensional porous crystals. Nano Letters. 22(2022): 3071-3076.
[4] U. Farooq. J. Teuwen, C. Dransfeld. Toughening of epoxy systems with interpenetrating polymer network (IPN): A review. MDPI-Polymers. 12(2020: 1908.
[5] G. Do, M. Geisselbrecht, W. Schwieger, H. Freund. Additive manufacturing of interpenetrating periodic open cellular structures (InterPOCS) with in operando adjustable flow characteristics. Chemical Engineering and Processing: Process Intensification. 148(2020): 107786.

[5.1] Y. Li, X. Chen, J. Zhou, X. Liu, D. Zhang, F. Du, W. He, P. Jia, H. Liu. A review of high-velocity impact on fiber-reinforced textile composites: potential for aero engine applications. International Journal of Mechanical Systems Dynamics. 2(2022): 50-64.
[6] G. R. Keiser, K. Fan, X. Zhang, R. D. Averitt. Towards dynamic, tunable, and nonlinear metamaterials via near field interactions: a review. Journal of Infrared, Millimeter, and Terahertz Waves. 34(2013): 709-723.
[7] N. Raina, R. Rani, A. Khan, K. Nagpal, M. Gupta. Interpenetrating polymer network as a pioneer drug delivery system: a review. Polymer Bulletin. 77(2020): 5027-5050.
[8] M. F. Ashby. The properties of foams and lattices. Philosophical Transactions of the Royal Society A. 364(2006): 15-30.
[9] L. Yang, O. Harrysson, D. Cormier, H. West, H. Gong, B. Stucker. Additive manufacturing of metal cellular structures: design and fabrication. TMS JOM. 67(2015), 3: 608-615.
[10] D. M. Correa, C. C. Seepersad, M. R. Haberman. Mechanical design of negative stiffness honeycomb materials. Integrating Materials and Manufacturing Innovation. 4(2015): 10.
[11] R. M. Christensen. Observations on the definition on yield stress. Acta Mechanica. 196(2008): 239-244.